0026-895X/09/7603-618–631$20.00
MOLECULAR PHARMACOLOGY
Copyright © 2009 The American Society for Pharmacology and Experimental Therapeutics
Mol Pharmacol 76:618–631, 2009

Vol. 76, No. 3
55152/3507319
Printed in U.S.A.

Biochemical and Electrophysiological Characterization of Almorexant, a Dual Orexin 1 Receptor (OX_1)/Orexin 2 Receptor (OX_2) Antagonist: Comparison with Selective OX_1 and OX_2 Antagonists

Pari Malherbe, Edilio Borroni, Emmanuel Pinard, Joseph G. Wettstein, and Frédéric Knoflach

CNS Research (P.M., E.B., J.G.W., F.K.) and Chemistry Discovery (E.P.), F. Hoffmann-La Roche Ltd., Basel, Switzerland

Received January 29, 2009; accepted June 17, 2009

ABSTRACT

Recent preclinical and clinical research has shown that almorexant promotes sleep in animals and humans without disrupting the sleep architecture. Here, the pharmacology and kinetics of [^{3}H]almorexant binding to human orexin 1 receptor (OX_1)- and human orexin 2 receptor (OX_2)-human embryonic kidney 293 membranes were characterized and compared with those of selective OX_1 and OX_2 antagonists, including 1-(5-(2-fluoro-phenyl)-2-methyl-thiazol-4-yl)-1-((*S*)-2-(5-phenyl-(1,3,4)oxadiazol-2-ylmethyl)-pyrrolidin-1-yl)-methanone (SB-674042), 1-(6,8-difluoro-2-methyl-quinolin-4-yl)-3-(4-dimethylamino-phenyl)-urea (SB-408124), and *N*-ethyl-2-[(6-methoxy-pyridin-3-yl)-(toluene-2-sulfonyl)-amino]-*N*-pyridin-3-ylmethyl-acetamide (EMPA). The effect of these antagonists was also examined in vitro on the spontaneous activity of rat ventral tegmental area (VTA) dopaminergic neurons. [^{3}H]Almorexant bound to a single saturable site on hOX_1 and hOX_2 with high affinity (K_d of 1.3 and 0.17 nM, respectively). In Schild analyses using the [^{3}H]inositol phosphates assay, almorexant acted as a competitive antagonist at hOX_1 and as a noncompetitive-like antagonist at hOX_2. In binding kinetic analyses, [^{3}H]almorexant had fast association and dissociation rates at hOX_1, whereas it had a fast association rate and a remarkably slow dissociation rate at hOX_2. In the VTA, orexin-A potentiated the basal firing frequency to 175 ± 17% of control in approximately half of the neurons tested. In the presence of 1 μM SB-674042 or SB-408124, the effect of orexin-A was only partially antagonized. However, in the presence of 1 μM EMPA or 1 μM almorexant, the effect of orexin-A was completely antagonized. In conclusion, almorexant exhibited a noncompetitive and long-lasting pseudo-irreversible mode of antagonism as a result of its very slow rate of dissociation from OX_2. The electrophysiology data suggest that OX_2 might be more important than OX_1 in mediating the effect of orexin-A on slow-firing of VTA dopaminergic neurons.

A preliminary account of some of the results has been published in abstract form [Knoflach F, Borroni E, Kratzeisen C, Marcuz A, Humbel U, Weber M, Zenner MT, Pinard E, Wettstein JG, and Malherbe P (2008) Biochemical and electrophysiological characterization of a dual OX_1R/OX_2R antagonist, almorexant and its comparison with the selective OX_1R and OX_2R antagonists SB-674042 and EMPA. *Soc Neurosci Abstr* **34:**826.817].

Article, publication date, and citation information can be found at http://molpharm.aspetjournals.org.
doi:10.1124/mol.109.055152.

Orexins (also called hypocretins) belong to a family of neuropeptides that are exclusively synthesized in the neuronal cell bodies of the lateral hypothalamic areas. Orexin-A/hypocretin-1 (33 amino acids) and orexin-B/hypocretin-2 (28 amino acids) are derived from the proteolytic processing of 130 amino acid polypeptide prepro-orexin (de Lecea et al.,

ABBREVIATIONS: OX_1, orexin 1 receptor; OX_2, orexin 2 receptor; ACT-078573, almorexant, (2*R*)-2-{(1*S*)-6,7-dimethoxy-1-[2-(4-trifluoromethyl-phenyl)-ethyl]-3,4-dihydro-1H-isoquinolin-2-yl}-*N*-methyl-2-phenyl-acetamide; CHO, Chinese hamster ovary; REM, rapid eye movement; IP, inositol phosphates; HEK, human embryonic kidney; FLIPR, fluorometric imaging plate reader; DA, dopamine; EMPA, *N*-ethyl-2-[(6-methoxy-pyridin-3-yl)-(toluene-2-sulfonyl)-amino]-*N*-pyridin-3-ylmethyl-acetamide; SB-674042, 1-(5-(2-fluoro-phenyl)-2-methyl-thiazol-4-yl)-1-((*S*)-2-(5-phenyl-(1,3,4)oxadiazol-2-ylmethyl)-pyrrolidin-1-yl)-methanone; Cp-2, 1-(9-oxo-8-trifluoromethyl-1,2,3,9-tetrahydro-pyrrolo[2,1-*b*]quinazolin-3-yl)-1-((*S*)-1-phenyl-ethyl)-3-(2-trifluoromethoxy-phenyl)-urea; Cp-3, 2-methyl-5-phenyl-thiazole-4-carboxylic acid cyclobutyl-[3-(4-fluoro-phenoxy)-propyl]-amide; Cp-4, 2-[[4-chloro-2-(hydroxy-phenyl-methyl)-phenyl]-(3,4-dimethoxybenzenesulfonyl)-amino]-*N*-methyl-acetamide; Cp-5, ((*S*)-1-(6,7-dimethoxy-3,4-dihydro-1H-isoquinolin-2-yl)-3,3-dimethyl-2-[(pyridin-4-ylmethyl)-amino]-butan-1-one; SB-334867, 1-(2-methyl-benzoxazol-6-yl)-3-[1,5]naphthyridin-4-yl-urea hydrochloride; SB-408124, 1-(6,8-difluoro-2-methyl-quinolin-4-yl)-3-(4-dimethylamino-phenyl)-urea; JNJ-10397049, 1-(2,4-dibromophenyl)-3-[(4S,5S)-2,2-dimethyl-4-phenyl-1,3-dioxan-5-yl]urea; VTA, ventral tegmental area; HBSS, Hanks' balanced salt solution; BSA, bovine serum albumin; DMSO, dimethyl sulfoxide; ACSF, artificial cerebrospinal fluid; CRC, concentration-response curve; NSB/TB%, nonspecific binding/total bound radioactivity; Cp-1, (2*R*)-2-{(1*S*)-6,7-dimethoxy-1-[2-(6-trifluoromethyl-pyridin-3-yl)-ethyl]-3,4-dihydro-1H-isoquinolin-2-yl}-*N*-methyl-2-phenyl-acetamide.

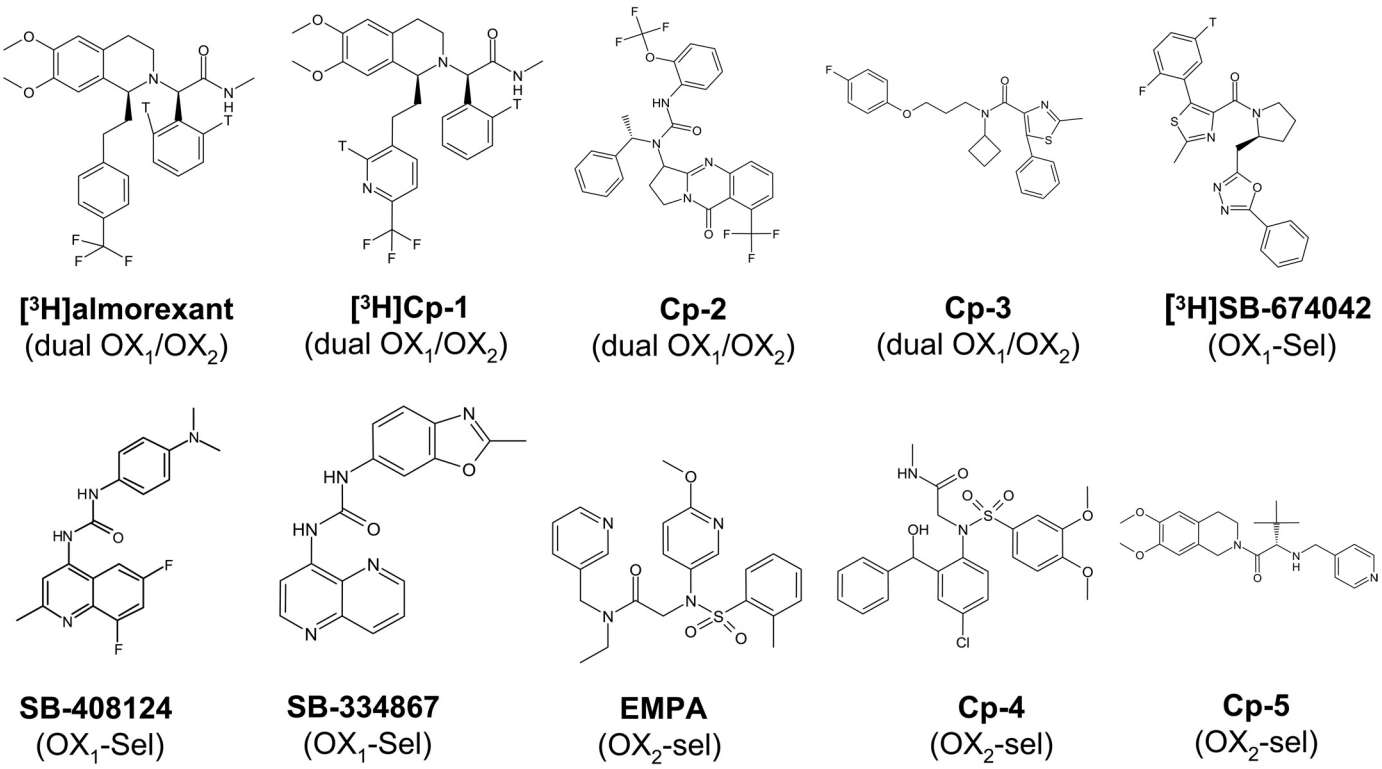

Fig. 1. Chemical structures of the selective OX_1, OX_2, and dual OX_1/OX_2 antagonists. T, tritium.

1998; Sakurai et al., 1998). They elicit their effect through two G-protein-coupled receptors called OX_1 (hypocretin receptor type 1) and OX_2 (hypocretin receptor type 2). Both OX_1 and OX_2 are coupled via $G_{q/11}$ to the activation of phospholipase C, leading to an elevation of intracellular Ca^{2+} levels (Sakurai et al., 1998). Moreover, OX_2 also couples via G_s and $G_{i/o}$ to the cAMP pathways (Tang et al., 2008). The [^{125}I]orexin-A binding and functional assays demonstrated that orexin-A has a 10-fold greater affinity for OX_1 over OX_2, whereas orexin-A and -B bind with similar affinity to OX_2 (Sakurai et al., 1998). Although both OX_1 and OX_2 are expressed in most brain regions, including ventral tegmental area (VTA), dorsal raphe nucleus, laterodorsal tegmental nuclei, pedunculopontine tegmental nuclei, and hypothalamus, OX_1 is most abundantly expressed in the locus ceruleus, whereas OX_2 is expressed in the regions controlling arousal, found abundantly in the tuberomammillary nucleus (Trivedi et al., 1998; Marcus et al., 2001).

Orexins and their receptors have been implicated in numerous physiological functions, including energy homeostasis, feeding and reward, and regulation of arousal and the sleep–wake cycle (Kilduff and Peyron, 2000; Ohno and Sakurai, 2008). Because of their depolarizing actions on distinct populations of monoaminergic neurons (Soffin et al., 2004), OX_1 and OX_2 might have different functions within the central nevous system. Several lines of evidence support the pivotal role of OX_2 in the regulation of sleep-wakefulness: a mutation (*canarc-1*), which disrupts the gene encoding OX_2, was found to be responsible for canine narcolepsy (Lin et al., 1999); furthermore, intracerebroventricular administration of orexin-A had no effect in narcoleptic dogs, although it significantly increased wakefulness in control dogs (Nishino et al., 2001). The orexin-induced wakefulness is largely mediated by the histaminergic system through OX_2 and is almost completely absent in H_1 receptor knockout mice (Huang et al., 2001; Yamanaka et al., 2002). Both OX_2 and H_1 receptors are localized in the tuberomammillary nucleus neurons, an important site for the regulation of sleep-wakefulness. OX_2 knockout mice exhibited abnormal attacks of non-REM sleep, marked sleep-wake fragmentation, and cataplexy (Willie et al., 2003). The selective stimulation of OX_2 by [Ala^{11}]orexin-B (100-fold selectivity for OX_2 over OX_1) promoted wakefulness in freely behaving rats (Akanmu and Honda, 2005). Conversely, a role for OX_1 in feeding and reward and in mediating some of the effects of drugs of abuse has been suggested (Harris et al., 2005; Thorpe and Kotz, 2005; Narita et al., 2006). The lateral hypothalamic orexin neurons project to reward-associated brain regions, including the nucleus accumbens and VTA, which suggests the involvement of orexins in drug-seeking and other motivational behaviors (Harris et al., 2005; Scammell and Saper, 2005). It is noteworthy that morphine-induced place preference seen in wild-type mice was abolished in mice lacking the prepro-orexin gene. The selective OX_1 antagonist SB-334867A, injected in the VTA, was able to block the morphine-conditioned place preference in rats (Narita et al., 2006). The biochemical characterization of an OX_2 antagonist, EMPA, with 900-fold selectivity in binding for OX_2 over OX_1 has been reported (Malherbe et al., 2009).

Preclinical (dog and rat) and phase I (healthy male subjects, single dose) investigations have shown that the dual

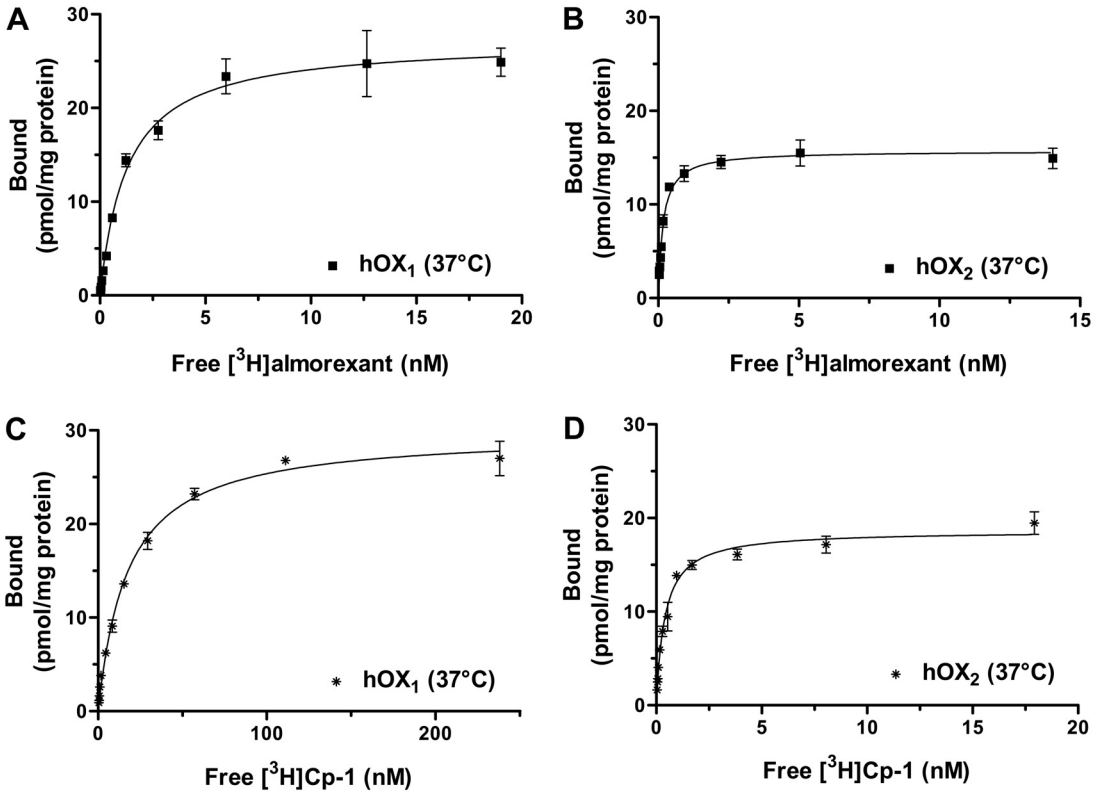

Fig. 2. Binding characteristic of [^{3}H]almorexant and [^{3}H]Cp-1 to hOX_1 and hOX_2 cell membranes. Saturation binding curves of [^{3}H]almorexant and [^{3}H]Cp-1 bindings to membrane from HEK293 cells transfected transiently with hOX_1 (A and C) or with hOX_2 (B and D). Each data point is the mean ± S.E. (bars) of three independent experiments performed in triplicate. The data were analyzed by nonlinear regression analysis using GraphPad Prism 4.0 software and a single-site binding model.

antagonist almorexant (ACT-078573), when administered orally during the active period, promoted sleep (non-REM and REM) in animals and humans without disrupting the sleep architecture or inducing cataplexy (Brisbare-Roch et al., 2007), thereby further validating the involvement of orexin system in the regulation of alertness and sleep. Here, the pharmacology and kinetics of [^{3}H]almorexant binding to human OX_1- and OX_2-expressing membranes were characterized. The antagonistic mechanism of almorexant was determined by Schild analyses using the orexin-A- or orexin-B-induced accumulation of [^{3}H]inositol phosphates (IP) assay in hOX_1- or hOX_2-expressing cells. Dopaminergic neurons of the VTA receive a dense projection of orexin neurons from the lateral hypothalamus (Fadel and Deutch, 2002) and are excited by orexin-A (Korotkova et al., 2003). To define the precise role of OX_1 and OX_2 in the modulation of VTA DA neurons, we conducted electrophysiological recordings in rat midbrain slices. The effects of almorexant, SB-674042, SB-408124 (Langmead et al., 2004), and EMPA on the spontaneous action potential firing of VTA DA neurons were compared.

Materials and Methods

Materials. Almorexant (ACT-078573; Brisbare-Roch et al., 2007), EMPA, SB-674042 (Langmead et al., 2004), Cp-1, Cp-2, Cp-3, Cp-4, and Cp-5 (Hirose et al., 2003) were synthesized in the Chemistry Department of F. Hoffmann-La Roche according to procedures described in patent literature. [^{3}H]Almorexant (specific activity, 42.7 Ci/mmol), [^{3}H]CP-1 (specific activity, 39.1 Ci/mmol), and [^{3}H]SB-674042 (specific activity, 24.4 Ci/mmol) were synthesized by Drs. Philipp Huguenin and Thomas Hartung at the Roche Chemical and Isotope Laboratories (Basel, Switzerland). SB-334867, SB-408124, orexin-A, and orexin-B were purchased from Tocris Bioscience (Bristol, UK). *myo*-[1,2-^{3}H]Inositol with PT6–271 stabilizer (specific activity, 16.0 Ci/mmol) and yttrium silicate RNA binding beads were purchased from GE Healthcare (Chalfont St. Giles, Buckinghamshire, UK).

Plasmids, Cell Culture, and Membrane Preparation. cDNA encoding human OX_1 (accession no. O43613) and human OX_2 (accession no. O43614) were subcloned into pCI-Neo expression vectors (Promega, Madison, WI). HEK293 cells were transfected as described previously (Malherbe et al., 2009). Forty-eight hours after transfection, cells were harvested and washed three times with cold phosphate-buffered saline and frozen at −80°C. The pellet was suspended in ice-cold buffer containing 15 mM Tris-HCl, pH 7.5, 2 mM

TABLE 1

[^{3}H]Almorexant and [^{3}H]Cp-1 binding properties at hOX_1 and hOX_2 and [^{3}H]SB-674042 binding at hOX_1

Saturation binding isotherms of [^{3}H]almorexant, [^{3}H]Cp-1, and [^{3}H]SB-674042 were performed on membrane preparations from HEK293 cells transiently transfected with hOX_1 or hOX_2 as described under *Materials and Methods*. The K_d and B_{max} values are mean ± S.E., calculated from three independent experiments (each performed in triplicate).

Radioligand and Receptor	K_d	B_{max}
	nM	*pmol/mg protein*
[^{3}H]Almorexant (37°C)		
hOX_1	1.3 ± 0.1	27.2 ± 0.6
hOX_2	0.17 ± 0.01	15.72 ± 0.2
[^{3}H]Cp-1 (37°C)		
hOX_1	17.52 ± 1.3	29.83 ± 0.7
hOX_2	0.40 ± 0.04	18.64 ± 0.5
[^{3}H]SB-674042 (23°C)		
hOX_1	0.74 ± 0.07	13.76 ± 0.38

$MgCl_2$, 0.3 mM EDTA, 1 mM EGTA, protease inhibitor cocktail EDTA-free (Roche Applied Science, Rotkreuz, Switzerland) and homogenized with a Polytron (Kinematica AG, Basel, Switzerland) for 30 s at 16,000 rpm. After centrifugation at 48,000*g* for 30 min at 4°C, the pellet was suspended in ice-cold buffer containing 75 mM Tris-HCl, pH 7.5, 12.5 mM $MgCl_2$, 0.3 mM EDTA, 1 mM EGTA, 250 mM sucrose, and protease inhibitor cocktail, EDTA-free. The membrane homogenate was frozen at −80°C before use.

[^{3}H]Almorexant, [^{3}H]Cp-1, and [^{3}H]SB-674042 Bindings. After thawing, membrane homogenates were centrifuged at 48,000*g* for 10 min at 4°C, the pellets were resuspended in the binding buffer (1× HBSS, 20 mM HEPES, pH 7.4, and 0.1% BSA) to a final assay concentration of 5 μg of protein/well. Saturation isotherms were determined by the addition of various concentrations of [^{3}H]almorexant (0.02–20 nM at OX_1, 0.03–15 nM at OX_2R), [^{3}H]Cp-1 (0.4–240 nM at OX_1, 0.03–18 nM at OX_2) or [^{3}H]SB-674042 (0.03–15 nM at OX_1) to these membranes (in a total reaction volume of 500 μl). The incubation for OX_1- and OX_2-expressing membranes were 60 and 120 min at 37°C, respectively, for both [^{3}H]almorexant and [^{3}H]Cp-1. The incubation time for [^{3}H]SB-674042 on OX_1 membranes was 90 min at 23°C. At the end of incubation, membranes were filtered onto unit-filter (96-well white microplate with bonded GF/C filter preincubated for 1 h in wash buffer plus 0.5% polyethylenimine and 0.1% BSA) with a Filtermate 196 harvester (PerkinElmer Life and Analytical Sciences, Waltham, MA) and washed four times with ice-cold wash buffer (1× HBSS and 20 mM HEPES, pH 7.4). Nonspecific bindings for [^{3}H]almorexant, [^{3}H]Cp-1, and [^{3}H]SB-674042 were measured in the presence of 10 μM almorexant, Cp-1, and SB-674042, respec-

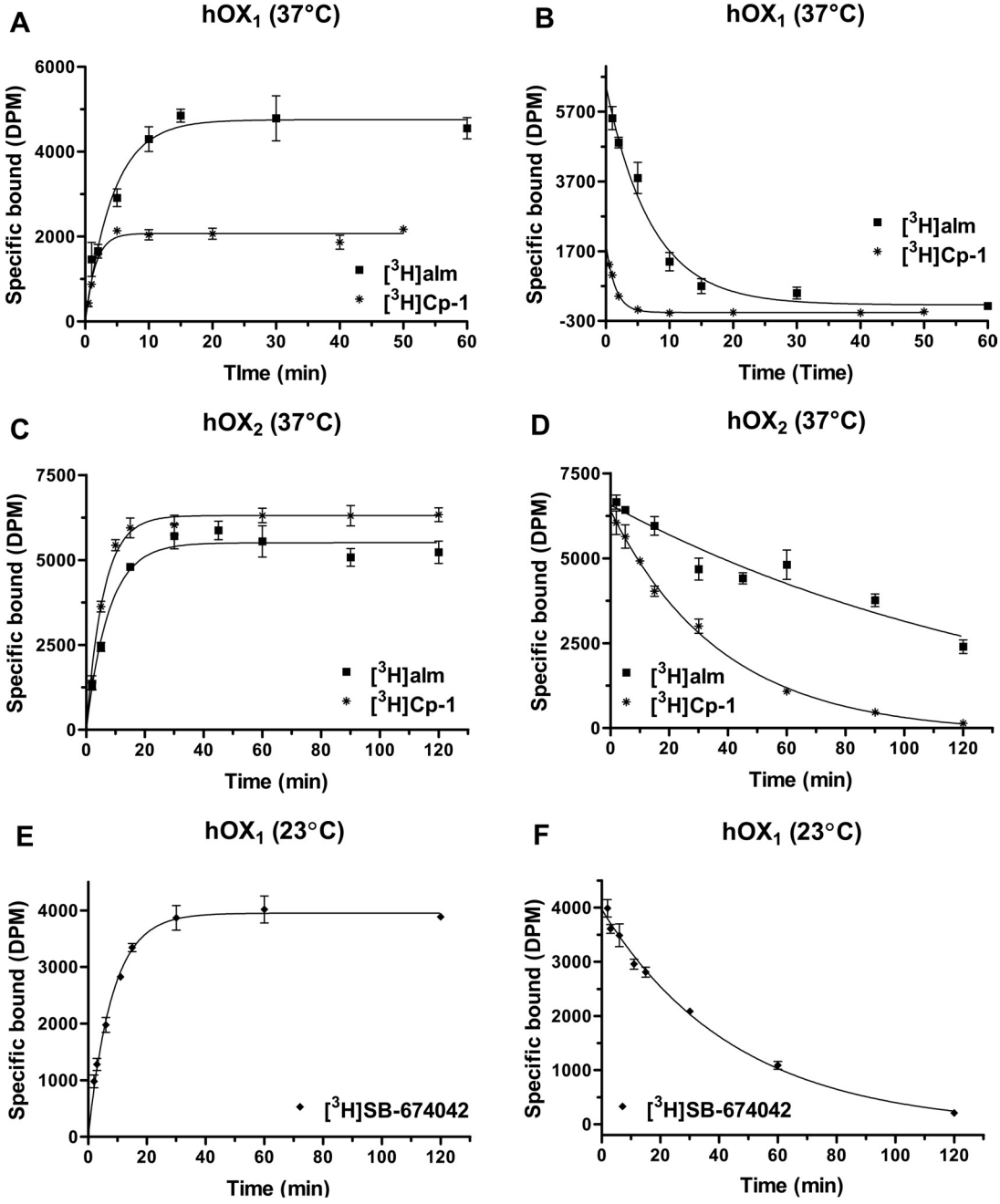

Fig. 3. Kinetics time course for the association (A, C, and E) and dissociation (B, D, and F) of [^{3}H]almorexant and [^{3}H]Cp-1 binding to hOX_1 and hOX_2 membranes and of [^{3}H]SB-674042 binding to hOX_1 membrane. Each data point is the mean ± S.E. (bars) of three independent experiments performed in quadruplet.

tively. Radioactivity on the filter was counted (5 min) on a Top-Count microplate scintillation counter (PerkinElmer Life and Analytical Sciences) with quenching correction after the addition of 45 μl of MicroScint 40 (PerkinElmer Life and Analytical Sciences) and shaking for 1 h. Saturation experiments were analyzed by Prism 4.0 (GraphPad Software, Inc., San Diego, CA) using the rectangular hyperbolic equation derived from the equation of a bimolecular reaction and the law of mass action, $B = (B_{max} \cdot [F])/(K_d + [F])$, where B is the amount of ligand bound at equilibrium, B_{max} is the maximum number of binding sites, $[F]$ is the concentration of free ligand, and K_d is the ligand dissociation constant. For inhibition experiments, membranes were incubated with [^{3}H]almorexant at a concentration equal to K_d value of radioligand and 10 concentrations of the inhibitory compound (0.0001–10 μM). IC_{50} values were derived from the inhibition curve and the affinity constant (K_i) values were calculated using the Cheng-Prussoff equation, $K_i = IC_{50}/(1+[L]/K_d)$, where $[L]$ is the concentration of radioligand, and K_d is its dissociation constant at the receptor, derived from the saturation isotherm. The association and dissociation kinetics for [^{3}H]almorexant, [^{3}H]Cp-1, and [^{3}H]SB-674042 were measured as described previously (Malherbe et al., 2009). Binding kinetics parameters, K_{ob} and K_{off} values (observed on and off rates), were derived from association-dissociation curves using the one-phase exponential association and decay equations (Prism 4.0; GraphPad Software), respectively. K_{on}, half-life, and K_d were calculated using the $K_{on} = (K_{ob} - K_{off})/[\text{ligand}]$, $t_{1/2} = \ln 2/K$, and $K_d = K_{off}/K_{on}$ equations, respectively.

[^{3}H]IP Accumulation Assay. [^{3}H]Inositol phosphates accumulation was measured as described previously (Malherbe et al., 2009) with the following adaptations. The Chinese hamster ovary (dHFr$^-$) mutant cell line stably expressing OX_1 or OX_2, CHO(dHFr$^-$)-OX_1 or CHO(dHFr$^-$)-OX_2, were maintained in Dulbecco's modified Eagle's medium (1×) with GlutaMax1, 4500 mg/l D-glucose and sodium pyruvate, 5% dialyzed fetal calf serum, 100 μg/ml penicillin, and 100 μg/ml streptomycin. Cells were washed twice in labeling medium: Dulbecco's modified Eagle's medium without inositol (MP Biomedicals, Irvine, CA), 10% dialyzed fetal calf serum, 1% penicillin/streptomycin, and 2 mM glutamate. Cells were seeded at 8×10^4 cells/well in poly(D-lysine)-treated 96-well plates in the labeling medium supplemented with 5 μCi/ml *myo*-[1,2-^{3}H]inositol and were incubated overnight. The following day, cells were washed three times with the wash buffer (1× HBSS and 20 mM HEPES, pH 7.4) and then incubated for 10 min at room temperature in assay buffer (1× HBSS, 20 mM HEPES, pH 7.4, 0.1% BSA, plus 8 mM LiCl final, to prevent phosphatidyl-inositide breakdown) before the addition of agonists or antagonists. When present, antagonists were incubated for 20 min at 37°C before stimulation with agonist; concentrations ranged from 0.00003 to 3 μM for orexin-A or orexin-B. After 45-min incubation at 37°C with agonist, the assay was terminated by the aspiration of the assay buffer and the addition of 100 μl of 20 mM formic acid to the cells. After shaking for 30 min at 23°C, a 40-μl aliquot was mixed with 80 μl of yttrium silicate beads (12.5 mg/ml) that bind to the inositol phosphates (but not inositol) and shaken for 30 min at 23°C. Assay plates were centrifuged for 2 min at 750*g* before counting on a Packard Top Count microplate scintillation counter with quenching correction (PerkinElmer Life and Analytical Sciences).

Intracellular Ca^{2+} Mobilization Assay. The CHO(dHFr$^-$)-OX_1 and -OX_2 stable cells lines were seeded at 5×10^4 cells/well in the poly(D-lysine)-treated, 96-well, black/clear-bottomed plates. Twenty-four hours later, the cells were loaded for 1 h at 37°C with 4 μM Fluo-4 acetoxymethyl ester in FLIPR buffer (1× HBSS, 20 mM HEPES, and 2.5 mM probenecid). Cells were washed five times with FLIPR buffer to remove excess dye, and then intracellular calcium mobilization ($[Ca^{2+}]_i$)was measured using a Fluorometric Imaging Plate Reader (FLIPR-96; Molecular Devices, Sunnyvale, CA) as described previously (Malherbe et al., 2009). Orexin-A (50 mM stock solution in DMSO) was diluted in FLIPR buffer plus 0.1% BSA. The EC_{50} and EC_{80} values of orexin were measured daily from standard agonist concentration-response curves in CHO(dHFr$^-$)-OX_1 or -OX_2 stable cell line. Inhibition curves were determined by the addition of 11 concentrations (0.0001–10 μM in FLIPR buffer) of inhibitory compounds and using EC_{80} value of orexin-A as agonist (a concentration that gave 80% of maximum agonist response, determined daily). The antagonists were applied 25 min (incubation at 37°C) before the application of the agonist. Responses were measured as peak increase in fluorescence minus basal, normalized to the maximal stimulatory effect induced by EC_{80} value of orexin-A. Inhibition curves were fitted according to the Hill equation $y = 100/(1 + (x/IC_{50})^{nH})$, where n_H is the slope factor using Prism 4.0 (GraphPad Software). K_b values were calculated according to the following equation: $K_b = IC_{50}/(1 + [A]/EC_{50})$, where A is the concentration of agonist added that is very close to agonist EC_{80} value, and IC_{50} and EC_{50} values were derived from the antagonist inhibition and orexin agonist curves, respectively.

Electrophysiology in Rat Midbrain Slices. Wistar rats (12–27 days old) were anesthetized in a 2.5% isoflurane/96.5% oxygen mixture for 2 min and decapitated, according to the approved procedure by the local institutional animal welfare committee. The brain was quickly removed, and horizontal midbrain slices (250 μm thick) containing the VTA were cut with a vibratome (Leica, Wetslar, Germany) in an ice-cold solution containing 250 mM glycerol, 2.5 mM KCl, 1.2 mM $MgCl_2$, 2.4 mM $CaCl_2$, 1.2 mM NaH_2PO_4, 26 mM $NaHCO_3$, and 11 mM D-glucose (335 mOsM). Immediately after cutting, the slices were transferred for 20 min to warm artificial cerebrospinal fluid (ACSF; 35°C) containing 119.0 mM NaCl, 2.5 mM KCl, 1.3 mM $MgCl_2$, 2.5 mM $CaCl_2$, 1 mM NaH_2PO_4, 26.2 mM $NaHCO_3$, and 11 mM D-glucose gassed with a mixture of 95% O_2/5% CO_2 (295 mOsM) and then stored for later use at room temperature. For electrophysiological recordings, a slice was transferred to the recording chamber (volume, ~1 ml) containing gassed ACSF held at 35°C and perfused at a rate of 2 ml/min. Neurons were identified visually using a microscope equipped with infrared differential interference contrast optics (Olympus, Basel, Switzerland). Loose

TABLE 2

Kinetic binding parameters for association and dissociation of [^{3}H]almorexant and [^{3}H]Cp-1 in hOX_1 and hOX_2 membranes and of [^{3}H]SB-674042 in the hOX_1 membranes

The K_{ob}, K_{off}, K_{on}, $t_{1/2}$, and K_d values are mean ± S.E. calculated from three independent experiments (each performed in quadruplet) as described under *Materials and Methods*.

Radioligand and Receptor	Association Kinetic			Dissociation Kinetic		Apparent K_d
	K_{ob}	K_{on}	$t_{1/2}$	K_{off}	$t_{1/2}$	
	min^{-1}	$nM^{-1} \cdot min^{-1}$	*min*	min^{-1}	*min*	*nM*
[^{3}H]Almorexant (37°C)						
hOX_1	0.225 ± 0.02	0.051 ± 0.01	3.07 ± 0.23	0.140 ± 0.01	4.95 ± 0.22	2.73 ± 0.23
hOX_2	0.130 ± 0.01	0.064 ± 0.00	5.34 ± 0.37	0.007 ± 0.00	104.60 ± 4.56	0.10 ± 0.01
[^{3}H]Cp-1 (37°C)						
hOX_1	0.628 ± 0.03	0.024 ± 0.00	1.11 ± 0.04	0.550 ± 0.02	1.25 ± 0.04	22.66 ± 1.12
hOX_2	0.171 ± 0.01	0.047 ± 0.00	4.07 ± 0.15	0.027 ± 0.01	26.15 ± 3.43	0.56 ± 0.24
[^{3}H]SB-674042 (23°C)						
hOX_1	0.122 ± 0.01	0.033 ± 0.01	5.71 ± 0.61	0.022 ± 0.01	31.57 ± 3.0	0.66 ± 0.15

patch recordings were made from presumed DA neurons that spontaneously fired action potentials, using thin-wall borosilicate glass pipette (Clark GCT150; Warner Instruments, Hamden, CT) filled with ACSF. Signals were filtered (1-Hz high and 2-KHz low pass) and amplified with a Multiclamp 700A amplifier (Molecular Devices) digitized at 10 kHz with a DigiData 1200 interface and stored on a personal computer with the pClamp 8.0 data acquisition software (both from Molecular Devices). A neuron was considered dopaminergic if it had a regular firing pattern (0.5–2 Hz), a broad (>2 ms) triphasic action potential (Grace and Onn, 1989), and was sensitive to quinpirole (100 nM), a dopamine receptor agonist. Action potentials were detected by means of threshold search using the Clampfit analysis program (Molecular Devices). The firing frequencies (action potentials per second) were calculated in bins of 1 min. Values are given as mean ± S.E.M., and n represents the number of neurons recorded. In concentration-response experiments, increasing concentrations of orexin-A or quinpirole were perfused in a consecutive manner. For each concentration, maximum firing frequencies were measured and plotted as a function of the concentration. Firing frequencies from each recorded neuron were fitted with the nonlinear least-squares fitting routine of the data analysis program Origin (OriginLab Corp, Northampton, MA) using the equation $f(x) = f_{max}/[1 + (x/EC_{50})^{n_H}]$, where f is the measured firing frequency, f_{max} is the maximum firing frequency, x is the concentration tested, EC_{50} is the half-maximum effective concentration, and n_H is the slope factor. Quinpirole concentration-response curves were normalized to the maximum firing frequency. In concentration-response shift experiments, concentration-response curves of orexin-A were generated after incubation of the slices with almorexant for at least 1 h. Drugs were applied to the slices by exchanging the solution of the recording chamber until a maximum effect was reached. All salts for ACSF solutions were obtained from Sigma-Aldrich (Basel, Switzerland). Stock solutions of EMPA, almorexant, SB-408124, and SB-

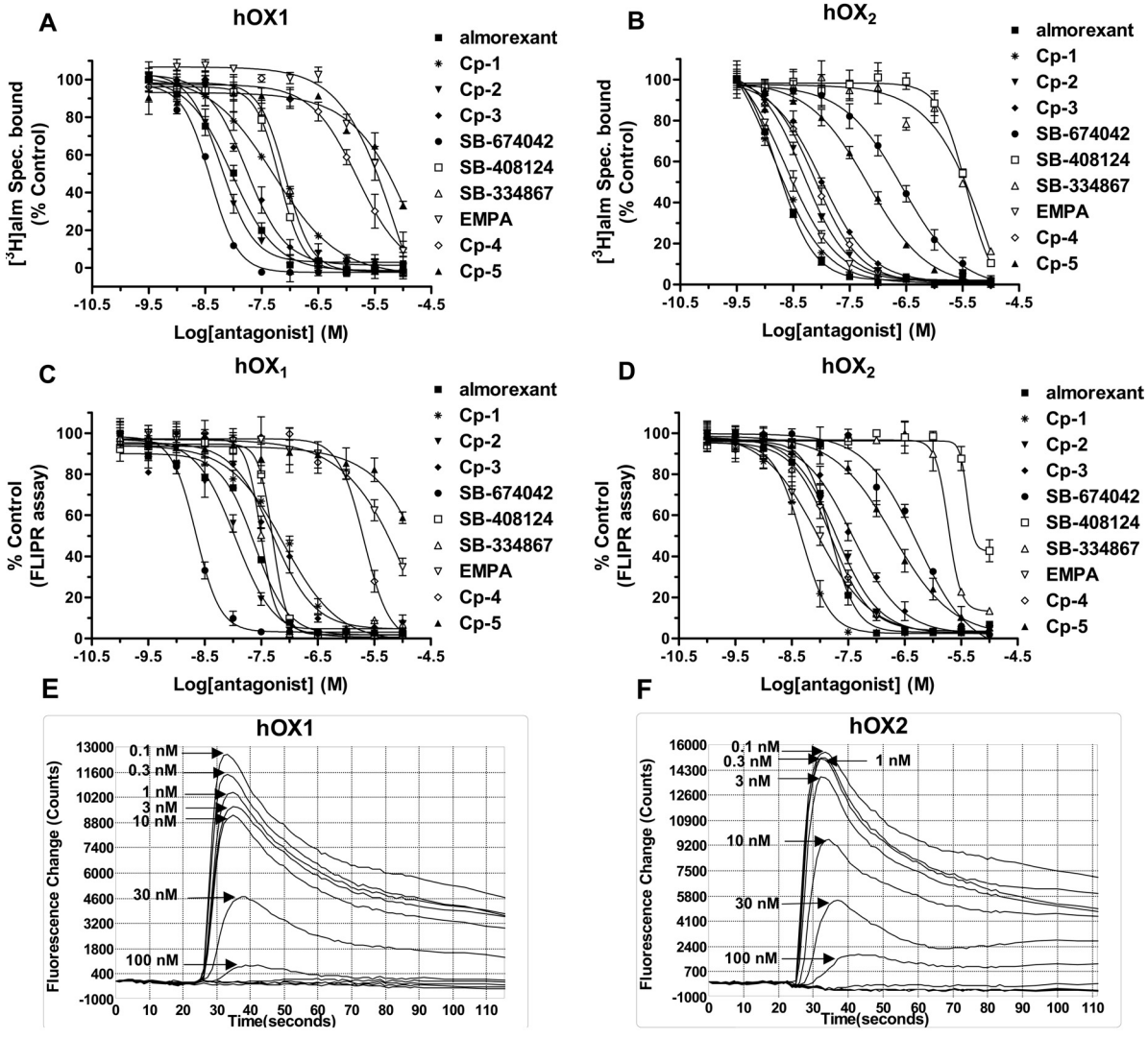

Fig. 4. Pharmacological profile of the orexin receptor antagonists. A and B, potencies of various selective OX_1, OX_2, and dual OX_1/OX_2 antagonists in the inhibition of [^{3}H]almorexant binding to the membrane preparations from HEK293 cells transiently expressing hOX_1 or hOX_2. [^{3}H]Almorexant was used at a concentration equal to its K_d values of 1.3 and 0.17 nM at hOX_1 and hOX_2, respectively, in these competition binding experiments. Each data point is the mean ± S.E. (bars) of three independent experiments performed in duplicate. C and D, concentration-dependent inhibition of orexin-A (EC_{80} value) stimulated increases in $[Ca^{2+}]_i$ by selective OX_1, OX_2, and dual OX_1/OX_2 antagonists at CHO(dHFr$^-$)-hOX_1 or -hOX_2 stable cell line as assayed using the Ca^{2+}-sensitive dye Flou-4 and a fluorometric imaging plate reader (FLIPR-96). Responses are normalized to the first control response. Each curve represents the mean ± S.E. (bars) of three independent concentration-response experiments (each performed in duplicate). E and F, multiple-well overlay (11 wells) of kinetics of representative tracings for the inhibition of actual orexin-A stimulated fluorescence responses by increasing concentrations of almorexant (0.1–10 000 nM) in the CHO(dHFr$^-$)-hOX_1 and -hOX_2 stable cell lines, respectively. Note that the cells were incubated with various concentrations of almorexant for 25 min at 37°C before the addition of orexin-A (EC_{80}), and then the fluorescence responses were measured immediately. The concentration of almorexant in each well is indicated by an arrow.

674042 (10 mM) were made in DMSO and diluted in gassed ACSF to reach a final concentration of DMSO never exceeding 0.1%.

Results

Binding Characteristics of [^{3}H]Almorexant and [^{3}H]Cp-1 and Their Comparison with [^{3}H]SB-674042. Almorexant (ACT-078573) is a dual OX antagonist. It was previously reported to potently inhibit the binding of [^{125}I]orexin-A to both OX_1 and OX_2 overexpressed in CHO cells with IC_{50} values of 6.6 and 3.4 nM, respectively, by using a whole-cell binding assay (Brisbare-Roch et al., 2007). In the present study, almorexant and its close analog Cp-1 were tritiated ([^{3}H]almorexant and [^{3}H]Cp-1) (Fig. 1). To characterize the in vitro binding of [^{3}H]almorexant and [^{3}H]Cp-1, saturation binding analyses were performed at binding equilibrium, as outlined under *Materials and Methods*, on membranes isolated from the HEK293 cells transiently transfected with hOX_1 and hOX_2. The saturation isotherms were monophasic and best-fitted to a one-site model for both radioligands at hOX_1 (Fig. 2, A and C) and hOX_2 (Fig. 2, B and D). The binding affinity of [^{3}H]almorexant to hOX_1 and hOX_2 membranes was temperature-dependent and increased substantially at 37°C. The dissociation constants (K_d) and the maximum number of binding sites (B_{max}) derived from the saturation isotherms are given in Table 1. At the K_d values, the percentage of nonspecific binding/total bound radioactivity (NSB/TB%) for [^{3}H]almorexant and [^{3}H]Cp-1 was approximately 15.1 and 16.5% at hOX_1 and 6.2 and 3.0% at hOX_2 for both radioligands, respectively.

Binding kinetics of [^{3}H]almorexant and [^{3}H]Cp-1 to membrane preparations from HEK293 cells transiently expressing hOX_1 or hOX_2 are shown in Fig. 3 and the kinetic parameters in Table 2. The association binding of [^{3}H]almorexant and [^{3}H]Cp-1 to hOX_1 was rapid with half-maximal binding occurring at 3 and 1.1 min and reaching equilibrium within 15 and 10 min, respectively (Fig. 3A). Likewise, the association kinetics of [^{3}H]almorexant and [^{3}H]Cp-1 to hOX_2 were fast with $t_{1/2}$ of 5.3 and 4.0 min, respectively, and reached equilibrium within 30 min for both radioligands (Fig. 3C). The data from both antagonists were fitted to a one-phase exponential model for hOX_1 and hOX_2 (Fig. 3, A and C, and Table 2).

The dissociation rates for [^{3}H]almorexant and [^{3}H]Cp-1 binding to hOX_1 and hOX_2 were determined by addition of an excess amount of unlabeled almorexant or Cp-1 after equilibrium was reached. The reversal of binding for [^{3}H]almorexant and [^{3}H]Cp-1 from hOX_1 membranes was complete with $t_{1/2}$ values of 5.0 and 1.3 min, respectively (Fig. 3B and Table 2). The rates of [^{3}H]almorexant and [^{3}H]Cp-1 dissociation from hOX_2 membranes were slow (Fig. 3D and Table 2). The calculations of the apparent K_d values derived from the

TABLE 3

Potencies of various selective OX_1, OX_2, and dual OX_1/OX_2 antagonists in the inhibition of [^{3}H]almorexant binding to the membrane preparations from HEK293 cells transiently expressing hOX_1 or hOX_2

K_i and n_H values for [^{3}H]almorexant binding inhibition by various antagonists were calculated as described under *Materials and Methods*. Values are mean ± S.E., calculated from three independent experiments (each performed in duplicate).

OX Antagonists	[^{3}H]Almorexant Competition Binding (37°C)			
	hOX_1		hOX_2	
	K_i	n_H	K_i	n_H
	nM		*nM*	
Almorexant	4.7 ± 0.9	1.1 ± 0.1	0.9 ± 0.0	1.3 ± 0.0
Cp-1	25.7 ± 1.8	0.8 ± 0.1	0.7 ± 0.0	1.0 ± 0.0
Cp-2	3.3 ± 0.8	1.5 ± 0.1	2.4 ± 0.1	1.1 ± 0.0
Cp-3	8.4 ± 2.2	1.3 ± 0.1	5.1 ± 0.4	1.0 ± 0.0
SB-674042	1.9 ± 0.5	1.8 ± 0.2	133.5 ± 53.0	0.8 ± 0.0
SB-408124	32.7 ± 1.8	2.1 ± 0.7	1850 ± 670.0	1.8 ± 0.5
SB-334867	41.6 ± 2.8	1.9 ± 0.1	6300.0 ± 2000.0	0.8 ± 0.0
EMPA	4533 ± 1580	0.9 ± 0.1	1.2 ± 0.1	1.0 ± 0.0
Cp-4	782.0 ± 212.0	1.1 ± 0.0	3.86 ± 0.3	1.1 ± 0.1
Cp-5	>10,000		33.4 ± 2.3	0.8 ± 0.0

TABLE 4

Potencies of various selective OX_1, OX_2, and dual OX_1/OX_2 antagonists on inhibition of orexin-A (EC_{80})-induced intracellular Ca^{2+} mobilization

IC_{50}, K_b, and n_H values for the inhibition of orexin-A (EC_{80})-evoked $[Ca^{2+}]_i$ response by various antagonists in the CHO(dHFr$^-$)-hOX_1 and hOX_2 stable cell lines were calculated as described under *Materials and Methods*. Values are mean ± S.E. calculated from three independent experiments (each performed in duplicate).

OX Antagonists	hOX_1			hOX_2		
	IC_{50}	K_b	n_H	IC_{50}	K_b	n_H
	nM			*nM*		
Almorexant	24.1 ± 5.2	3.3 ± 0.4	1.5 ± 0.5	15.6 ± 5.2	1.5 ± 0.2	1.9 ± 0.4
Cp-1	78.6 ± 6.7	10.8 ± 0.9	0.9 ± 0.1	4.8 ± 1.0	0.5 ± 0.1	1.8 ± 0.1
Cp-2	11.1 ± 2.4	2.7 ± 0.2	1.3 ± 0.2	19.3 ± 0.5	1.7 ± 0.1	1.1 ± 0.0
Cp-3	51.4 ± 4.0	4.7 ± 0.8	1.2 ± 0.1	37.6 ± 6.1	3.7 ± 0.7	1.0 ± 0.0
SB-674042	2.2 ± 0.2	0.5 ± 0.0	2.0 ± 0.4	531.0 ± 36.7	137.7 ± 9.5	0.9 ± 0.0
SB-408124	50.7 ± 3.2	12.4 ± 0.8	3.5 ± 0.8	4000.0 ± 2000.0	1037.0 ± 519.0	7.0 ± 3.0
SB-334867	31.3 ± 4.0	7.7 ± 1.2	3.3 ± 0.5	1870.0 ± 102.0	484.8 ± 26.5	3.9 ± 0.0
EMPA	>10,000			8.8 ± 1.7	0.8 ± 0.2	0.9 ± 0.0
Cp-4	2070.0 ± 150.0	507.3 ± 52.5	1.9 ± 0.5	15.6 ± 2.2	1.5 ± 0.2	1.3 ± 0.1
Cp-5	>10,000			198.0 ± 73.3	20.3 ± 7.1	0.8 ± 0.0

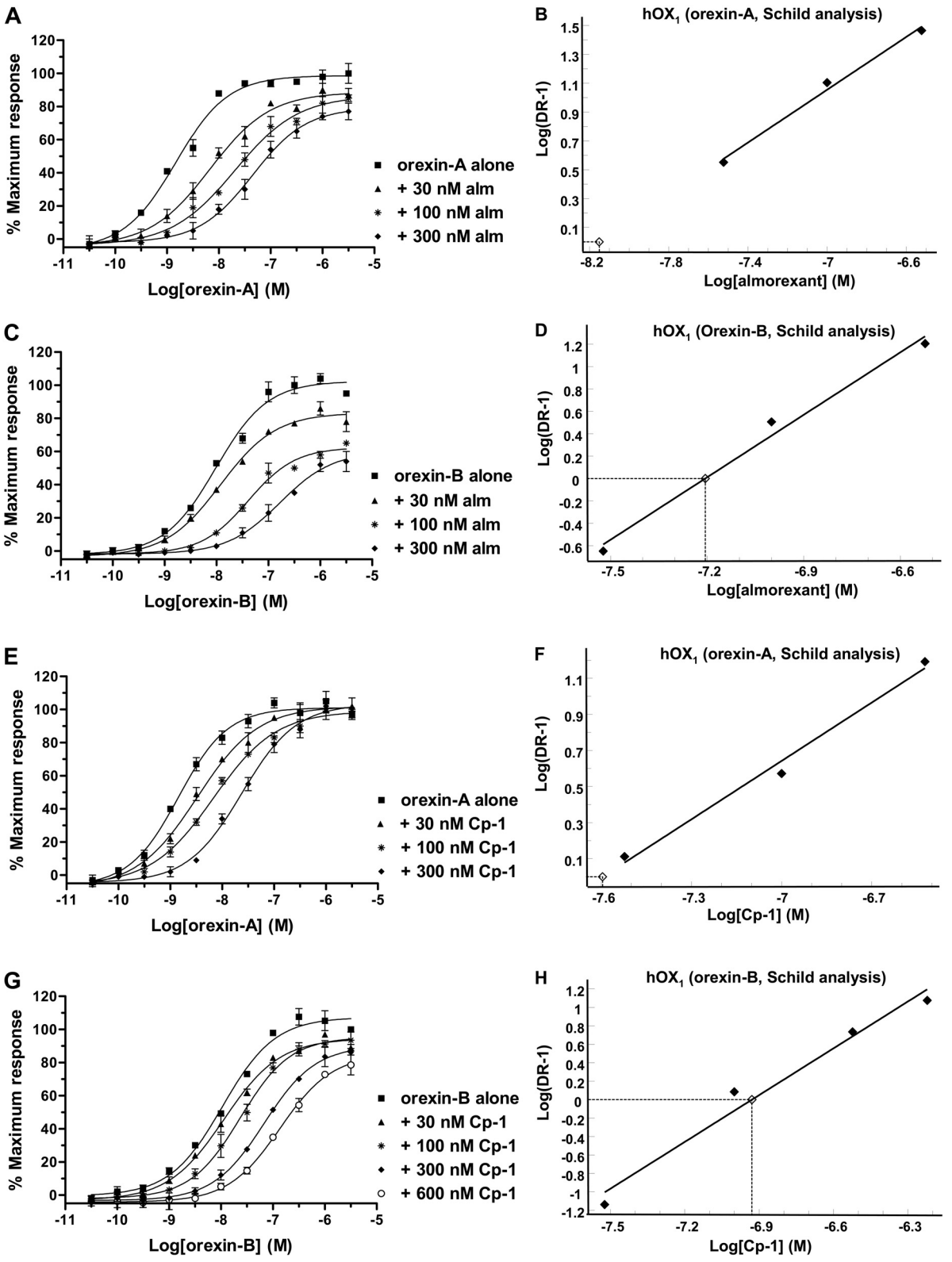

Fig. 5. Schild analyses showing the competitive mode of antagonism by almorexant and Cp-1 at hOX_1. CRCs for [^{3}H]IP formation stimulated by orexin-A and orexin-B in the absence or presence of increasing concentrations of almorexant (A and C) or Cp-1 (E and G) in CHO(dHFr$^-$)-hOX_1 stable cell line. Schild plots for antagonism by almorexant (B and D) and by Cp-1 (F and H). The EC_{50} values derived from orexin-A and orexin-B CRCs in the absence or presence of increasing concentrations of almorexant (A and C) or Cp-1 (E and G) were used to calculate the dose ratios (DR = EC_{50}/EC_{50}) and plotted according to Schild regression for almorexant in B and D or for Cp-1 in F and H. Each CRC is the mean ± S.E. (bars) of three independent experiments performed in quadruplet.

kinetic experiments are given in Table 2. The apparent K_d values of [^{3}H]almorexant and [^{3}H]Cp-1 at hOX_1 and hOX_2 were in good agreement with the equilibrium K_d values shown in Table 1.

[^{3}H]SB-674042, the first radioligand antagonist selective for hOX_1 to be described previously (Langmead et al., 2004), was used in the current study for comparison. [^{3}H]SB-674042 has been characterized previously in saturation and binding kinetics at hOX_1 with whole-cell and membrane-based scintillation proximity assays (Langmead et al., 2004). In current study with the filtration binding assay, [^{3}H]SB-674042 displayed a high-affinity binding to hOX_1 with a K_d value of 0.74 nM (Table 1). Binding of [^{3}H]SB-674042 to hOX_1 was rapid with half-maximal binding occurring after 5.7 min and reaching equilibrium within 30 min (Fig. 3E and Table 2). The dissociation rate for [^{3}H]SB-674042 binding to hOX_1 was determined by the addition of an excess amount of SB-674042 after equilibrium was reached. The reversal of binding for [^{3}H]SB-674042 was complete with a K_{off} value of 0.022 min^{-1} (Fig. 3F and Table 2). The apparent dissociation constant was 0.66 nM, which was similar to the equilibrium K_d value of 0.74 nM. The filtration binding data of [^{3}H]SB-674042 are in good agreement with those reported previously using whole-cell and scintillation proximity binding assays (Langmead et al., 2004).

Two different cell systems were used in the current study. HEK293 cells were transiently transfected with hOX_1 and hOX_2 and were used for binding studies, and CHO(dHFr$^-$)-hOX_1 and -hOX_2 stable cells were used for functional studies (FLIPR and IP accumulation assays). Because HEK293 cells were adapted to grow and to be transiently transfected in suspension in spinner flasks, it was possible to produce and prepare large quantities of transfected cells and membranes required for binding studies. As discussed previously for [^{3}H]EMPA (Malherbe et al., 2009), saturation binding experiments with membranes prepared from HEK293-hOX_1 and -hOX_2 and from CHO(dHFr$^-$)-hOX_1 and -hOX_2 cells showed similar K_d values for [^{3}H]SB-674042 binding (0.74 versus 1.4 nM at hOX_1) and for [^{3}H]EMPA binding (1.1 versus 0.7 nM at hOX_2) on these membranes, respectively. The only difference between these two cell systems were B_{max} values (14 versus 0.98 pmol/mg protein at hOX_1 and 38 versus 2.4 pmol/mg protein at hOX_2, respectively) and NSB/TB% (3.8 versus 23% at hOX_1 and 1.3 versus 11% at hOX_2, respectively) that indicated a higher level of expression and lower NSB/TB% in HEK293 cells than that of CHO cells. Therefore, HEK293 cells were used for binding studies.

Pharmacological Assessment of [^{3}H]Almorexant in Competition Binding to hOX_1 and hOX_2 Membranes. To assess the pharmacological profile of [^{3}H]almorexant in competition binding assay, selective OX_1 and OX_2 and dual OX_1/OX_2 antagonists were synthesized, which had been described previously in the patent literature. The chemical structures of various OX antagonists used in current study, the selective OX_1 antagonists SB-334867 (Smart et al., 2001), SB-408124 (Langmead et al., 2004) and SB-674042 (Langmead et al., 2004); the selective OX_2 antagonists EMPA (Malherbe et al., 2009), Cp-4, and Cp-5 (Hirose et al., 2003); and the dual OX_1/OX_2 antagonists almorexant (Brisbare-Roch et al., 2007), Cp-1, Cp-2, and Cp-3 are shown in Fig. 1. Potencies of these antagonists in inhibiting [^{3}H]almorexant binding to HEK293-hOX_1 and -hOX_2 cell membranes are shown in Fig. 4, A and B, with their derived K_i and n_H values in Table 3.

Potencies of Various OX Antagonists on Inhibition of Orexin-A-Evoked $[Ca^{2+}]_i$ Response. In CHO(dHFr$^-$)-hOX_1 and -hOX_2 stable cell lines, orexin-A (0.0001–10 μM) elicited a concentration-dependent increase in intracellular free calcium $[Ca^{2+}]_i$ with EC_{50} and n_H values of 0.4 ± 0.1 nM and 1.0 ± 0.1, and 0.5 ± 0.1 nM and 0.7 ± 0.1, respectively, as monitored using the Ca^{2+}-sensitive dye Fluo-4 and a fluorometric imaging plate reader (FLIPR-96). To compare the antagonism potency of various OX antagonists in [^{3}H]almorexant competition binding and functional FLIPR assays, the concentration-dependent inhibition of orexin-A (EC_{80} value)-evoked increases in $[Ca^{2+}]_i$ by the selective OX_1- and OX_2- and the dual OX_1/OX_2 antagonists in hOX_1- and hOX_2-expressing cells are shown in Fig. 4, C and D, with their derived IC_{50}, K_b and n_H values in Table 4. To show the time course of fluorescence changes in each well, the traces of the actual calcium fluorescence responses for the inhibition of orexin-A stimulated increase in $[Ca^{2+}]_i$ responses by almorexant in the CHO(dHFr$^-$)-hOX_1 and -hOX_2 stable cells are presented in Fig. 4, E and F, respectively.

Comparison of the Mode of Antagonism of OX Antagonists at hOX_1 and hOX_2. To characterize the inhibition mode of OX antagonists, the concentration-response curves (CRCs) for [^{3}H]IP formation stimulated by orexin-A or orexin-B were measured in the absence or presence of increasing concentrations of antagonist in the CHO(dHFr$^-$)-hOX_1 and -hOX_2 stable cells lines. Orexin-A and orexin-B elicited concentration-dependent increases in the accumulation of [^{3}H]IP in the hOX_1-expressing cells with EC_{50} values of 1.4 and 11.0 nM and in the OX_2-expressing cells with EC_{50}

TABLE 5

Schild constants for antagonism of orexin-A- or orexin-B-induced accumulation of [^{3}H]IP by OX antagonists in the CHO(dHFr$^-$)-hOX_1

The apparent antagonist potency (pA_2) and Schild slope values were determined from Schild plot analyses shown in Fig. 5, B, D, F, and H.

OX Antagonist	Agonist	hOX_1			
		pA_2	K_b[a]	Schild Slope	Mode of Antagonism
			nM		
Almorexant	Orexin-A	8.15	7.10	0.92	Competitive
	Orexin-B	7.21	61.70	1.90	Competitive
Cp-1	Orexin-A	7.6	25.12	1.08	Competitive
	Orexin-B	6.93	117.50	1.69	Competitive
SB-674042	Orexin-A				Noncompetitive
SB-408124	Orexin-A				Noncompetitive
SB-334867	Orexin-A				Noncompetitive

values of 1.1 and 2.4 nM, respectively. When orexin-A was used as agonist, both almorexant and Cp-1 acted as competitive antagonists at hOX_1, shifting orexin-A CRCs to the right without changing its maximal response (Fig. 5, A and E). However, when orexin-B was used as agonist, increasing concentrations of almorexant and CP-1 produced a rightward shift along with a partial decrease of maximal response of the orexin-B CRCs (Fig. 5, C and G). The apparent antagonist potency (pA_2) and the Schild slope values calculated from orexin-A and orexin-B Schild analyses (Fig. 5, B, D, F, and H) are given in Table 5. As seen in Table 5, there is a good agreement between the functional potencies of almorexant and Cp-1 derived from FLIPR assay (K_b) (Table 4) and the [^{3}H]IP accumulation assay (K_b[a]) (Table 5). In addition, the selective OX_1 antagonists SB-674042, SB-408124, and SB-334867 displayed a noncompetitive-like mode of antagonism at hOX_1, shifting orexin-A CRCs to the right with a concomitant decrease in maximal response (Fig. 6, A–C). Likewise, as seen in Fig. 7, A–D, almorexant and Cp-1 behaved in a noncompetitive manner at hOX_2 and produced a rightward shift along with a full decline of maximal response of both orexin-A and orexin-B CRCs.

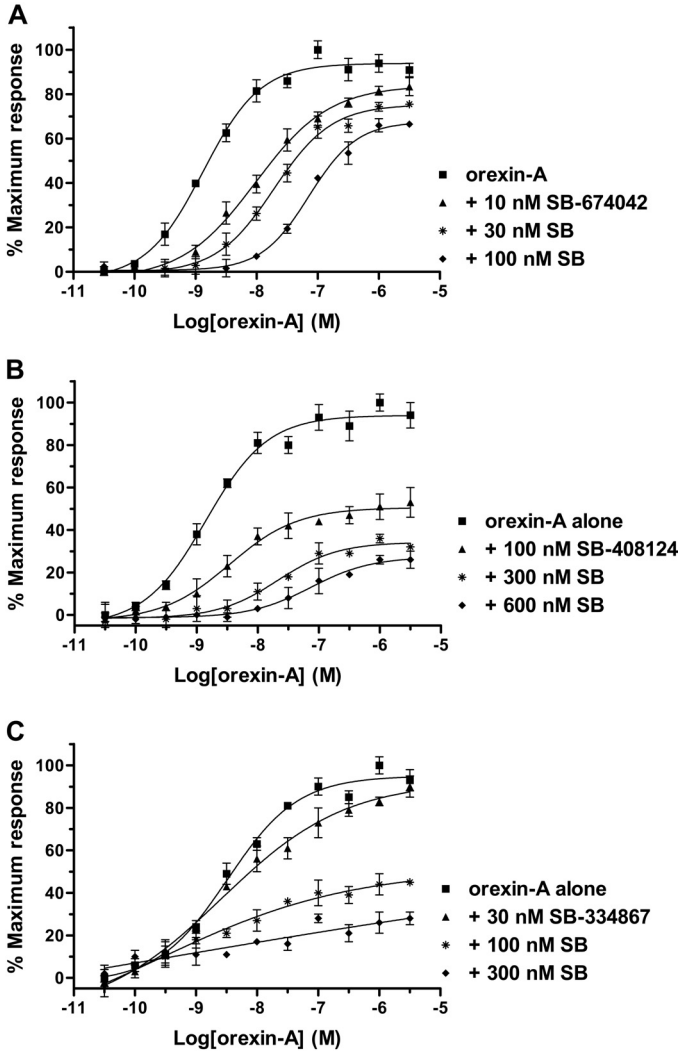

Fig. 6. Schild analyses showing the noncompetitive-like mode of antagonism by SB-674042, SB-408124, and SB-334867 at OX_1. CRCs for [^{3}H]IP formation stimulated by orexin-A in the absence or presence of increasing concentrations of SB-674042 (A), SB-408124 (B) or SB-334867 (C) in the CHO(dHFr$^-$)-hOX_1 stable cell line. Each CRC is the mean ± S.E. (bars) of three independent experiments performed in quadruplet.

Effect of OX Antagonists on Firing Frequency of Rat VTA DA Neurons. To assess the role of OX antagonists on native OX receptors in brain slices, we performed extracellular recordings of spontaneous activity of DA neurons in the VTA. It has been shown previously that a subset of VTA DA neurons is excited by orexin-A (Korotkova et al., 2003). These neurons can be identified on the basis of the regular firing frequency, action potential duration, and sensitivity to DA agonists and orexin-A. We first confirmed the dopaminergic nature of some of the recorded neurons. For this, quinpirole, a DA-selective agonist, was tested on inhibition of firing frequency (Fig. 8A). As expected, quinpirole concentration-dependently inhibited the activity of all neurons tested with an IC_{50} of 22 nM (n = 3). However, orexin-A (100 nM) produced an increase in firing frequency up to 175 ± 17% of control in 29 of 48 neurons. This is in keeping with the previously published study (Korotkova et al., 2003). In concentration-response experiments, orexin-A concentration-dependently increased the firing frequency of three neurons with an EC_{50} of 23 nM (Fig. 8B). To assess the effect of OX antagonists, a near-saturating concentration of orexin-A (100 nM) was used. We first established that repeated applications of orexin-A (100 nM) after complete recovery from the application elicited similar increases of the basal firing frequency without apparent desensitization (n = 4). As shown in Fig. 9A, application of almorexant (1 μM) to the slice did not change the basal firing frequency of a representative neuron. In the continuous presence of almorexant, orexin-A (100 nM) did not significantly enhance the basal firing frequency of the neurons after three applications anymore (Fig. 9B). The time course of antagonism of almorexant was rather slow: the complete reversal of the effect of orexin-A by almorexant occurred after 90 min of perfusion (Fig. 9B). In five neurons, the firing frequencies in the absence and presence of almorexant were 2.43 ± 0.80 and 2.52 ± 0.70 Hz, respectively. In the same neurons, the increase of firing frequency by orexin-A (100 nM) was 170 ± 29 and 105 ± 2% of control in the absence and presence of almorexant (1 μM), respectively (Table 6). The ability of almorexant to shift the concentration-response curve of orexin-A for increasing the firing frequency of DA VTA neurons was assessed. In slices incubated for 60 to 70 min with 100 nM almorexant, orexin-A was less potent and efficacious (Fig. 9C). The EC_{50} values for increase of firing frequencies by orexin-A in the absence and presence of almorexant were 29 (n = 5) and 68 nM (n = 6), respectively, and the increase of firing frequency by orexin-A (100 nM) in the absence and presence of almorexant was 269 ± 26 and 186 ± 29% of control, respectively. These experiments demonstrate the antagonistic property of almorexant on the orexin-A-induced increase of firing frequency of DA VTA neurons.

The effect of SB-408124, SB-674042, and EMPA (1 μM) on basal firing frequency and on orexin-A-induced increase of firing frequency was assessed using the same experimental paradigm. All three compounds had no effect on basal firing frequency (Table 6). EMPA completely reversed the effect of orexin-A. In contrast to almorexant and EMPA, SB-408124 and SB-674042 only partially reversed the effect of orexin-A on the firing frequency of VTA DA neurons (Table 6). The time course of the antagonism by EMPA and SB-408124 was

faster than that of almorexant, occurring already 20 min after perfusion of the compound (Fig. 10).

Discussion

Insomnia is the most common sleep disorder, affecting 20% of the general population and having a severe impact on quality of life. Current therapies that are mainly based on $GABA_A$ receptor modulation (Bhat et al., 2008) result in several side effects, including disruption of sleep architecture, insufficient sleep maintenance, withdrawal effects, and abuse potential (Roth and Roehrs, 1991). Recent positive clinical data with almorexant have indicated that this OX antagonist is efficacious in inducing and maintaining sleep without disrupting the sleep architecture (Brisbare-Roch et al., 2007). Thus, OX antagonists represent an alternative therapeutical approach for the treatment of insomnia (Nishino, 2007; Roecker and Coleman, 2008). In the present work, we have characterized the pharmacological profile of almorexant and its monoamide analog, Cp-1. [^{3}H]Almorexant and [^{3}H]Cp-1 bound with high affinity to a single saturable site on recombinant human OX_1 (K_d values of 1.3 ± 0.1 and 17.5 ± 1.3 nM at 37°C, respectively) and OX_2 (K_d values of 0.17 ± 0.01 and 0.40 ± 0.04 nM at 37°C, respectively). It is noteworthy that Cp-1 displayed a 14-fold decrease in binding affinity at hOX_1, yet only a 2.4-fold decrease at hOX_2 compared with almorexant. As shown previously, the peptide agonist orexin-A distinctly recognizes OX_1 from OX_2 (Ammoun et al., 2003; Takai et al., 2006). It was concluded that orexin-A binding to OX_1 requires more molecular determinants than binding to OX_2. Therefore, as demonstrated in the present study with Cp-1, minor modifications in the chemical structure of almorexant are expected to have a more pronounced effect on the binding affinity of the modified compound to OX_1 than that to OX_2.

Binding kinetic analyses revealed that both [^{3}H]almorexant and [^{3}H]Cp-1 have fast association and dissociation rates at hOX_1, whereas they have a fast association and a slow dissociation rate at hOX_2 (the reversal of the binding for both antagonists was complete with a $t_{1/2}$ value of 105 and 26 min, at 37°C, for [^{3}H]almorexant and [^{3}H]Cp-1, respectively). The selective OX_1 and OX_2 and the dual OX_1/OX_2 antagonists displaced [^{3}H]almorexant binding with the following rank order of potencies: SB-674042>Cp-2>almorexant>Cp-3>Cp-1>SB-408124>SB-334667>Cp-4>EMPA>Cp-5 from HEK293-hOX_1 membranes and Cp-1>almorexant>EMPA>Cp-2>Cp-4>Cp-3>Cp-5>SB-674042>SB-408124>SB334867 from HEK293-hOX_2 membranes. These results are consistent with the rank order of potencies of these ligands in inhibiting orexin-A-evoked $[Ca^{2+}]_i$ response at hOX_1 and hOX_2.

Investigation of the antagonistic mechanism of almorexant and Cp-1 revealed that both compounds act as competitive antagonists at hOX_1 in the presence of orexin-A as agonist but display a tendency toward a partial noncompetitive like mode in the presence of orexin-B. As further evidence, the Schild slopes of 1.80 and 1.69 for almorexant and Cp-1 at OX_1, respectively, show a deviation from simple competitive antagonism with unit slope. However, almorexant and Cp-1 behaved in a noncompetitive manner at hOX_2. This mode of action, independent of the agonist used, was characterized by a rightward shift of the orexin-A or orexin-B concentration-response curves in the presence of increasing almorexant or Cp-1 concentrations with a concomitant large decrease in the maximal effect of orexin-A or orexin-B. A possible explanation for the noncompetitive-like antagonism of almorexant at hOX_2 determined by Schild plot analyses may be its remarkably slow dissociation rate from hOX_2 that was observed in the kinetic study. Because of almorexant's slow dissociation, a large portion of the OX_2 is not available for activation by orexin-A or orexin-B; consequently, the maximally achievable response of orexin-A or orexin-B decreases dramatically

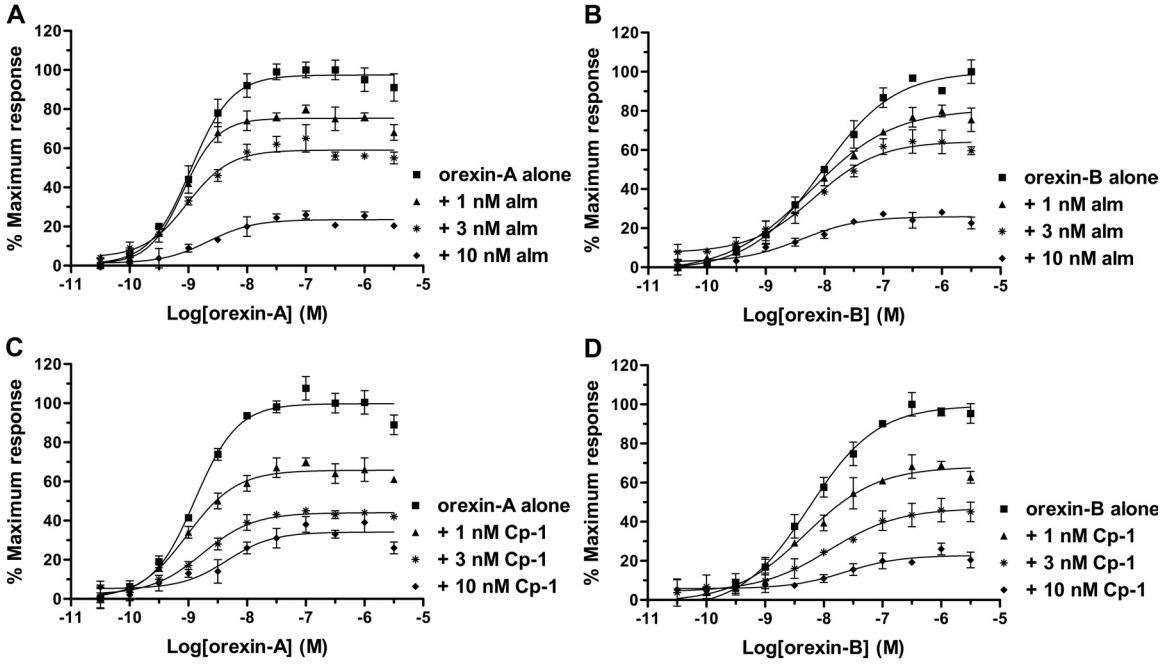

Fig. 7. Schild analyses showing the noncompetitive-like mode of antagonism by almorexant and Cp-1 at OX_2. CRCs for [^{3}H]IP formation stimulated by orexin-A and orexin-B in the absence or presence of increasing concentrations of almorexant (A and B) or Cp-1 (C and D) in CHO(dHFr$^-$)-hOX_2 stable cell line. Each CRC is the mean ± S.E. (bars) of three independent experiments performed in quadruplet.

in comparison to fast dissociating antagonist. Schild plot analyses of the OX_1 antagonists SB-33486, SB-408124, and SB-674042 (with 63-, 84- and 275-fold selectivity in FLIPR assay for hOX_1 over hOX_2, respectively) showed that all behaved in a noncompetitive like manner at hOX_1, similarly to that of almorexant at hOX_2. The noncompetitive-like mode of antagonism of these compounds was also characterized by a very steep hill slope (n_H values of 3.3, 3.5, and 2.0 for SB-33486, SB-408124, and SB-674042, respectively) observed in the FLIPR assay using hOX_1-expressing cells. The binding kinetics of [^{3}H]SB-674042 further demonstrated that SB-674042 has a slow dissociation rate (the reversal of the binding was complete with a $t_{1/2}$ value of 32 min, at 23°C) at hOX_1, which could also account for its noncompetitive-like mode of antagonism observed in the orexin-A-evoked accumulation of [^{3}H]IP assay.

Neurons containing orexins from the lateral hypothalamus strongly innervate the ventral tegmental area (Fadel and Deutch, 2002; Baldo et al., 2003), and electrophysiological recordings have shown previously that both orexin-A and orexin-B increase the firing rate of VTA neurons (Korotkova et al., 2003). Although orexins act on two types of VTA neurons, dopaminergic (characterized by slow firing frequency of ~2.2 Hz and broad action potential of >2 ms) and GABAergic (characterized by rapid firing frequency of ~7.3 Hz and brief action potential of <1.5 ms), yet they preferentially activate VTA dopamine (A10) neurons projecting to the nucleus accumbens and prefrontal cortex (Korotkova et al., 2003). In the current study, the effect of OX antagonists almorexant, SB-408124, SB-674042, and EMPA on firing frequency of rat VTA DA neurons were examined by loose-patch electrophysiological technique. In the VTA, the majorities of neurons fired action potentials with a slow frequency and were sensitive to quinpirole, a D_2 receptor agonist. Orexin-A increased the basal firing frequency of responsive DA VTA neurons in concentration-response experiments, with an EC_{50} of 23 nM. A value of the same order of magnitude has been reported previously (78 nM) (Korotkova et al., 2003). In the present study, only approximately half of the DA neurons examined were responsive to orexin-A. A recent study demonstrated that orexin neurons preferentially activate caudomedial ventral tegmental area dopamine neurons (Vittoz et al., 2008). Because we did not select DA neurons from this particular subregion of the VTA, it is very possible that a certain number of the recorded neurons were not responsive to orexin-A.

The OX antagonists tested in this study had no intrinsic effect on the spontaneous activity of VTA DA neurons. Almorexant completely reversed the effect of orexin-A on the

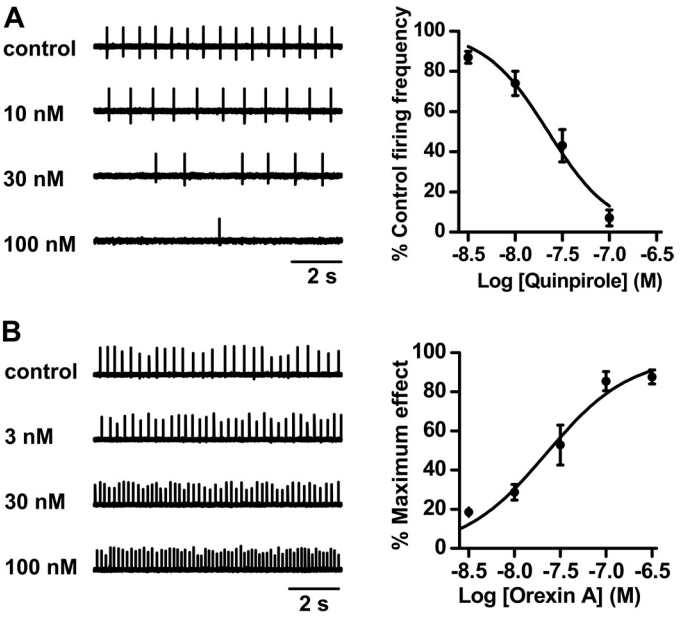

Fig. 8. Effect of quinpirole and orexin-A on the firing frequency of DA neurons in the VTA. Quinpirole inhibits (A) and orexin-A increases (B) the spontaneous activity of representative neurons. The traces on the left were recorded in the absence (control) and presence of the indicated concentrations of the drugs. Concentration-response curves on the right represent the decrease or increase in firing frequency plotted as a function of concentration of the drugs. Points indicate mean responses normalized to the maximum effect (orexin-A) or expressed as a percentage of the baseline activity (quinpirole) of all neurons tested at the indicated concentration. The sigmoid curves are a nonlinear fit of the points generated using the logistic equation (see *Materials and Methods*).

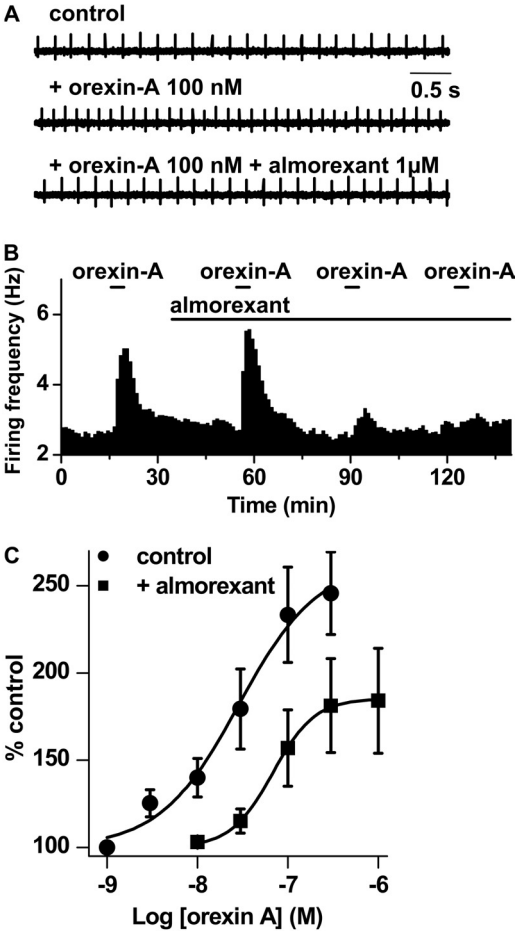

Fig. 9. Almorexant completely antagonizes the effect of orexin-A on firing frequency of DA VTA neurons. A, spontaneous activity of a VTA neuron recorded in the absence (control) and presence of orexin-A and orexin-A with almorexant. B, firing frequency plotted as a function of time. The average firing frequency was calculated over 1-min intervals. The small horizontal bars indicate the duration of bath applications of 100 nM orexin-A. The long horizontal bar indicates the duration of application of almorexant (1 μM). Note that the effect of orexin-A reversed to baseline upon wash-off. C, concentration-response relationships for increase of firing frequency of DA VTA neurons by orexin-A obtained in the absence and presence of 100 nM almorexant. Points indicate the mean ± S.E.M. firing frequency expressed as a percentage of baseline activity. The sigmoid curves are nonlinear fits of the points generated using the logistic equation (see *Materials and Methods*).

firing frequency of DA neurons in the VTA. This was achieved with a saturating concentration (1 μM) of almorexant blocking both OX_1 and OX_2. In concentration-response shift experiments performed at a lower almorexant concentration (100 nM), a rightward shift of the orexin-A CRC along with a decrease of maximal response was observed. This noncompetitive behavior of almorexant is in good agreement with its pseudo-irreversible mode of antagonism at OX_2, which is seen in Schild plot analyses using the [^{3}H]IP assay and in OX_2 binding kinetic studies. EMPA (a highly potent and selective OX_2) (Malherbe et al., 2009) did also completely reverse the increase in firing frequency of these neurons. However, at the concentration tested, this antagonist acts only at OX_2. This suggests that OX_2 are sufficient to mediate the excitatory effects of orexin neurons on the VTA DA neurons. This complex behavior of selective OX antagonist in the VTA neurons might well indicate the formation of heterodimers/oligomers by both receptors. Indeed, the residue hOX_2-Val308 (corresponds to hOX_1-Val302, located on the transmembrane 6 on the outer surface of the receptor) seems to be involved in OX_2 dimerization, and the 1246G>A polymorphism (substitution of valine 308 by isoleucine) of the OX_2 gene has been suggested to modulate the genetic risk for cluster headaches by interfering with this dimerization process (Rainero et al., 2008). Furthermore, a report investigating the coexpression of OX_1 and cannabinoid CB1 has shown that the heterodimerization of OX_1-CB1 receptors resulted in both ligand-dependent and -independent coordinated alterations of receptor localization and function (Ellis et al., 2006).

It is noteworthy that a recent investigation comparing almorexant, SB-408124, and the selective OX_2 antagonist JNJ-10397049 in sleep modulation in rats has demonstrated that although both JNJ-10397049 and almorexant induced and prolonged sleep time (non-REM and REM), the selective OX_2 antagonist had a 10-fold higher potency than dual OX_1/OX_2 antagonist. On the contrary, SB-408124 had no effect on any sleep parameter tested, and it attenuated the sleep-promoting effect of OX_2 antagonist when it was coadministered with JNJ-10397049 (Dugovic et al., 2009).

In the present study, the OX_1-selective antagonists SB-408124 and SB-674042 only partially reversed the effect of orexin-A. However, in vivo administration of the OX_1 antagonist SB-334867 blocked the locomotor sensitization to cocaine and occluded the cocaine-induced potentiation of excitatory currents in VTA dopamine neurons (Borgland et al., 2006). Therefore, the lesser contribution of OX_1 on orexin-A-mediated increase of firing frequency in the VTA can still account for robust in vivo effects. It has been hypothesized that orexin neurons may play an important role in modulating the reward process (Harris and Aston-Jones, 2006). Thus, in addition to a remedy for sleep disorders, selective OX antagonists might also be promising molecules for the treatment of addiction. In conclusion, almorexant exhibited a noncompetitive and long-lasting pseudo-irreversible mode of antagonism as a result of its very slow rate of dissociation from OX_2. The electrophysiology data suggest that OX_2 might be more important than OX_1 in mediating the effect of orexin-A on slow firing of VTA dopaminergic neurons.

TABLE 6
Effect of OX_1 and OX_2 antagonists on basal and orexin-A-induced increase of firing frequency of DA neurons in the VTA
All compounds were tested at 1 μM according to the experimental procedure shown in Fig. 9.

OX Antagonist	Basal Firing Frequency		Increase of Firing Frequency		Reversal of Orexin-A Effect	*n*
	Control	+ Antagonist	Orexin-A	Orexin-A + Antagonist		
	Hz		*% control*		*%*	
Almorexant	2.43 ± 0.8	2.52 ± 0.7	170 ± 29	105 ± 2	89 ± 5	5
EMPA	1.57 ± 0.34	1.45 ± 0.32	150 ± 20	104 ± 2	89 ± 7	6
SB-408124	2.89 ± 0.44	2.99 ± 0.37	161 ± 17	131 ± 14	62 ± 13	5
SB-674042	2.47 ± 0.48	2.47 ± 0.48	163 ± 8	129 ± 8	57 ± 9	5

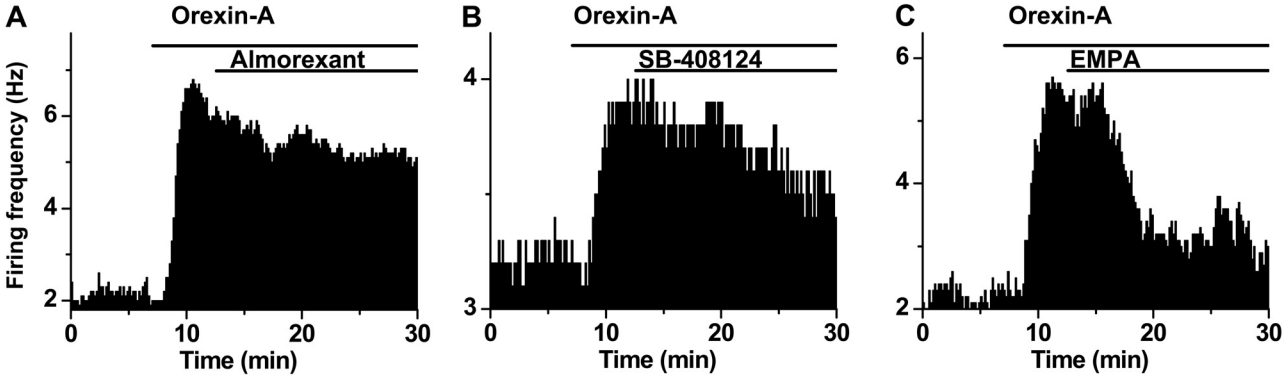

Fig. 10. Time course of the effect of almorexant, SB-408124, and EMPA in reversing the orexin-A-induced increase of firing frequency of DA VTA neurons. The firing frequencies of representative neurons are plotted as a function of time. The average firing frequency was calculated over 10-s intervals. Orexin-A (100 nM) was applied to the slice for the time indicated by the top bar. When a maximum effect of orexin-A was reached, the antagonists almorexant (A), SB-408124 (B), and EMPA (C) were applied at 1 μM to the slice for the time indicated by the bottom bars in the continuous presence of orexin-A. Note that in contrast to SB-408124 and EMPA, almorexant did not completely antagonize the effect of orexin-A within this short time period (20 min).

Acknowledgments

We are grateful to Valérie Goetschy, Marie-Laure Heusler, Urs Humbel, Claudia Kratzeisen, Anne Marcuz, Marie-Thérèse Miss, Michael Weber, and Marie-Thérèse Zenner for excellent technical assistance.

References

Akanmu MA and Honda K (2005) Selective stimulation of orexin receptor type 2 promotes wakefulness in freely behaving rats. *Brain Res* **1048:**138–145.
Ammoun S, Holmqvist T, Shariatmadari R, Oonk HB, Detheux M, Parmentier M, Akerman KE, and Kukkonen JP (2003) Distinct recognition of OX1 and OX2 receptors by orexin peptides. *J Pharmacol Exp Ther* **305:**507–514.
Baldo BA, Daniel RA, Berridge CW, and Kelley AE (2003) Overlapping distributions of orexin/hypocretin- and dopamine-beta-hydroxylase immunoreactive fibers in rat brain regions mediating arousal, motivation, and stress. *J Comp Neurol* **464:**220–237.
Bhat A, Shafi F, and El Solh AA (2008) Pharmacotherapy of insomnia. *Expert Opin Pharmacother* **9:**351–362.
Borgland SL, Taha SA, Sarti F, Fields HL, and Bonci A (2006) Orexin A in the VTA is critical for the induction of synaptic plasticity and behavioral sensitization to cocaine. *Neuron* **49:**589–601.
Brisbare-Roch C, Dingemanse J, Koberstein R, Hoever P, Aissaoui H, Flores S, Mueller C, Nayler O, van Gerven J, de Haas SL, et al. (2007) Promotion of sleep by targeting the orexin system in rats, dogs and humans. *Nat Med* **13:**150–155.
de Lecea L, Kilduff TS, Peyron C, Gao X, Foye PE, Danielson PE, Fukuhara C, Battenberg EL, Gautvik VT, Bartlett FS 2nd, et al. (1998) The hypocretins: hypothalamus-specific peptides with neuroexcitatory activity. *Proc Natl Acad Sci U S A* **95:**322–327.
Dugovic C, Shelton JE, Aluisio LE, Fraser IC, Jiang X, Sutton SW, Bonaventure P, Yun S, Li X, Lord B, et al. (2009) Blockade of orexin-1 receptors attenuates orexin-2 receptor antagonism-induced sleep promotion in the rat. *J Pharmacol Exp Ther* **330:**142–151.
Ellis J, Pediani JD, Canals M, Milasta S, and Milligan G (2006) Orexin-1 receptor-cannabinoid CB1 receptor heterodimerization results in both ligand-dependent and -independent coordinated alterations of receptor localization and function. *J Biol Chem* **281:**38812–38824.
Fadel J and Deutch AY (2002) Anatomical substrates of orexin-dopamine interactions: lateral hypothalamic projections to the ventral tegmental area. *Neuroscience* **111:**379–387.
Grace AA and Onn SP (1989) Morphology and electrophysiological properties of immunocytochemically identified rat dopamine neurons recorded in vitro. *J Neurosci* **9:**3463–3481.
Harris GC and Aston-Jones G (2006) Arousal and reward: a dichotomy in orexin function. *Trends Neurosci* **29:**571–577.
Harris GC, Wimmer M, and Aston-Jones G (2005) A role for lateral hypothalamic orexin neurons in reward seeking. *Nature* **437:**556–559.
Hirose M, Egashira S, Goto Y, Hashihayata T, Ohtake N, Iwaasa H, Hata M, Fukami T, Kanatani A, and Yamada K (2003) *N*-acyl 6,7-dimethoxy-1,2,3,4-tetrahydroisoquinoline: the first orexin-2 receptor selective non-peptidic antagonist. *Bioorg Med Chem Lett* **13:**4497–4499.
Huang ZL, Qu WM, Li WD, Mochizuki T, Eguchi N, Watanabe T, Urade Y, and Hayaishi O (2001) Arousal effect of orexin A depends on activation of the histaminergic system. *Proc Natl Acad Sci U S A* **98:**9965–9970.
Kilduff TS and Peyron C (2000) The hypocretin/orexin ligand-receptor system: implications for sleep and sleep disorders. *Trends Neurosci* **23:**359–365.
Korotkova TM, Sergeeva OA, Eriksson KS, Haas HL, and Brown RE (2003) Excitation of ventral tegmental area dopaminergic and nondopaminergic neurons by orexins/hypocretins. *J Neurosci* **23:**7–11.
Langmead CJ, Jerman JC, Brough SJ, Scott C, Porter RA, and Herdon HJ (2004) Characterisation of the binding of [^{3}H]-SB-674042, a novel nonpeptide antagonist, to the human orexin-1 receptor. *Br J Pharmacol* **141:**340–346.
Lin L, Faraco J, Li R, Kadotani H, Rogers W, Lin X, Qiu X, de Jong PJ, Nishino S, and Mignot E (1999) The sleep disorder canine narcolepsy is caused by a mutation in the hypocretin (orexin) receptor 2 gene. *Cell* **98:**365–376.
Malherbe P, Borroni E, Gobbi L, Knust H, Nettekoven M, Pinard E, Roche O, Rogers-Evans M, Wettstein J, and Moreau JL (2009) Biochemical and behavioural characterization of EMPA, a novel high-affinity, selective antagonist for the OX_2 receptor. *Br J Pharmacol* **156:**1326–1341.
Marcus JN, Aschkenasi CJ, Lee CE, Chemelli RM, Saper CB, Yanagisawa M, and Elmquist JK (2001) Differential expression of orexin receptors 1 and 2 in the rat brain. *J Comp Neurol* **435:**6–25.
Narita M, Nagumo Y, Hashimoto S, Narita M, Khotib J, Miyatake M, Sakurai T, Yanagisawa M, Nakamachi T, Shioda S, et al. (2006) Direct involvement of orexinergic systems in the activation of the mesolimbic dopamine pathway and related behaviors induced by morphine. *J Neurosci* **26:**398–405.
Nishino S (2007) The hypocretin/orexin receptor: therapeutic prospective in sleep disorders. *Expert Opin Investig Drugs* **16:**1785–1797.
Nishino S, Fujiki N, Yoshida Y, and Mignot E (2001) The effects of hypocretin-1 (orexin A) in hypocretin receptor 2 gene mutated and hypocretin ligand-deficient narcoleptic dogs. *Sleep* **24:**287A.
Ohno K and Sakurai T (2008) Orexin neuronal circuitry: role in the regulation of sleep and wakefulness. *Front Neuroendocrinol* **29:**70–87.
Rainero I, Gallone S, Rubino E, Ponzo P, Valfre W, Binello E, Fenoglio P, Gentile S, Anoaica M, Gasparini M, et al. (2008) Haplotype analysis confirms the association between the HCRTR2 gene and cluster headache. *Headache* **48:**1108–1114.
Roecker AJ and Coleman PJ (2008) Orexin receptor antagonists: medicinal chemistry and therapeutic potential. *Curr Top Med Chem* **8:**977–987.
Roth T and Roehrs TA (1991) A review of the safety profiles of benzodiazepine hypnotics. *J Clin Psychiatry* **52:**38–41.
Sakurai T, Amemiya A, Ishii M, Matsuzaki I, Chemelli RM, Tanaka H, Williams SC, Richardson JA, Kozlowski GP, Wilson S, et al. (1998) Orexins and orexin receptors: a family of hypothalamic neuropeptides and G protein-coupled receptors that regulate feeding behavior. *Cell* **92:**573–585.
Scammell TE and Saper CB (2005) Orexin, drugs and motivated behaviors. *Nat Neurosci* **8:**1286–1288.
Smart D, Sabido-David C, Brough SJ, Jewitt F, Johns A, Porter RA, and Jerman JC (2001) SB-334867-A: the first selective orexin-1 receptor antagonist. *Br J Pharmacol* **132:**1179–1182.
Soffin EM, Gill CH, Brough SJ, Jerman JC, and Davies CH (2004) Pharmacological characterisation of the orexin receptor subtype mediating postsynaptic excitation in the rat dorsal raphe nucleus. *Neuropharmacology* **46:**1168–1176.
Takai T, Takaya T, Nakano M, Akutsu H, Nakagawa A, Aimoto S, Nagai K, and Ikegami T (2006) Orexin-A is composed of a highly conserved C-terminal and a specific, hydrophilic N-terminal region, revealing the structural basis of specific recognition by the orexin-1 receptor. *J Pept Sci* **12:**443–454.
Tang J, Chen J, Ramanjaneya M, Punn A, Conner AC, and Randeva HS (2008) The signalling profile of recombinant human orexin-2 receptor. *Cell Signal* **20:**1651–1661.
Thorpe AJ and Kotz CM (2005) Orexin A in the nucleus accumbens stimulates feeding and locomotor activity. *Brain Res* **1050:**156–162.
Trivedi P, Yu H, MacNeil DJ, Van der Ploeg LH, and Guan XM (1998) Distribution of orexin receptor mRNA in the rat brain. *FEBS Lett* **438:**71–75.
Vittoz NM, Schmeichel B, and Berridge CW (2008) Hypocretin /orexin preferentially activates caudomedial ventral tegmental area dopamine neurons. *Eur J Neurosci* **28:**1629–1640.
Willie JT, Chemelli RM, Sinton CM, Tokita S, Williams SC, Kisanuki YY, Marcus JN, Lee C, Elmquist JK, Kohlmeier KA, et al. (2003) Distinct narcolepsy syndromes in orexin receptor-2 and orexin null mice: molecular genetic dissection of non-REM and REM sleep regulatory processes. *Neuron* **38:**715–730.
Yamanaka A, Tsujino N, Funahashi H, Honda K, Guan JL, Wang QP, Tominaga M, Goto K, Shioda S, and Sakurai T (2002) Orexins activate histaminergic neurons via the orexin 2 receptor. *Biochem Biophys Res Commun* **290:**1237–1245.

Address correspondence to: Dr. Pari Malherbe, F. Hoffmann-La Roche Ltd., Bldg. 69/333, CH-4070 Basel, Switzerland. E-mail: parichehr.malherbe@roche.com